Proc. of the 9th Intl. Conf. of Asian Society for Precision Engg. and Nanotechnology (ASPEN 2022)
15–18 November 2022, Singapore. Edited by Nai Mui Ling Sharon and A. Senthil Kumar
doi://10.3850/978-981-18-6021-8_OR-01-0075

Mechanical Performance of ER70S-6 Low-Carbon Steel Fabricated by Wire Arc Additive Manufacturing

Shibo Liu[1#], Peng Chen[1], Sun Xianchong[1#], Ang Joo Hock[2], Xiling Yao[1], Du Zhenglin[1] and Youxiang Chew[1],

1 Singapore Institute of Manufacturing Technology, 73 Nanyang Drive, 637662, Singapore
2 Sembcorp Marine Ltd. 80 Tuas South Boulevard, Singapore 637051

Corresponding Author: Liu Shibo/ Email: liu_shibo@simtech.a-star.edu.sg,
Sun Xianchong/ Email: Xianchong_sun@simtech.a-star.edu.sg,

KEYWORDS: Wire arc additive manufacturing, Cold metal transfer, low carbon steel

Wire arc additive manufacturing (WAAM) is well-recognized as an efficient wire-based deposition process for the repair and fabrication of large metallic parts. However, the cost of additive feedstock material remains a key barrier to the adoption of this additive manufacturing technology. In this study, a WAAM process of a low-cost, commonly used welding filler material, ER70S-6 low-carbon steel, was performed to assess the formability of bulk parts. The weld bead dimensions with varying cold metal transfer (CMT) parameters will be mapped and presented. Block samples were prepared using the optimized process parameters at a deposition rate of 4.3kg/hour. Experimental results showed that the hardness and tensile properties of as-deposited ER70S-6 are sensitive to the thermal conditions during the deposition process. Furthermore, Si-rich oxides segregations were observed in the cross-sectional analysis of as-deposited parts. The influences of these Si-enriched islands on the mechanical properties will be discussed. The investigation aims to contribute to more potential applications of WAAM processing of cost-effective low-carbon steel for the marine & offshore industry.

1. Introduction

Over the past decades, additive manufacturing (AM) has drawn growing interest from researchers and industries worldwide. Customized 3D components can be produced in a layer-by-layer manner by AM techniques using powder or wire feedstock [1]. Compared with the powder-based AM techniques that have been extensively studied and industrialized, wire arc additive manufacturing (WAAM) possesses the advantages of high deposition efficiency (up to 10 kg/h with WAAM [2] compared with typically 0.6 kg/h using powder-based AM [3]) and the relatively lower cost of wire feedstock which can be substantial, when considering the repair and fabrication of large-scale metallic components. WAAM can be executed via different welding techniques, such as gas metal arc welding (GMAW), gas tungsten arc welding (GTAW), and plasma arc welding (PAW) [4]. The cold metal transfer (CMT) is a variation based on GMAW developed by Fronius [5]. The heat input during welding is significantly reduced and coupled with precise droplet deposition, hence leading to reduced weld pool dimensions and spatters. The feasibility of CMT-WAAM processes has also been demonstrated by researchers using Inconel 718 superalloy and Al-6Mg alloy as feedstock materials [6, 7].

ER70S-6 steel is a well-known low-carbon steel with excellent welding properties and its WAAM formability has been reported by different research groups [8–11]. ER70S-6 parts fabricated by CMT-WAAM have also been reported recently [12]. However, there is a lack of studies on the effects of process output parameters with the input CMT process parameters. Moreover, as a low-carbon steel with Mn and Si, silicate islands tend to form on the surface of weld beads, and their inclusions can result in destabilization of the following deposition [13]. Consequently, the mechanical performance of ER70S-6 components composed of multiple weld beads may be affected by the accumulation of silicate islands. In this

study, the CMT-WAAM process of ER70S-6 steel is parametrically investigated through the dimensional responses of weld beads, followed by block deposition with interlayer oxide removal. The mechanical properties of the deposited samples are studied, and their correlations with the silicate islands and thermal conditions are discussed. The result of this study will aid the time-efficient production of ER70-S components with consistent mechanical performance.

2. Experiment

The ER70S-6 wire used in this study was provided by HYUNDAI WELDING with the nominal composition in Table 1. The diameter of the ER70S-6 wire is 1.2 mm. An ABB robot arm equipped with a Fronius TPS/400i CMT system was employed to conduct the CMT-WAAM experiments. All experiments were carried out on EH36 steel substrates with shielding gas composed of 82% Argon and 18% CO_2.

Table 1. Nominal composition of the ER70S-6 wire

Element	C	Si	Mn	P	S	Fe
wt. %	0.07	0.83	1.48	0.011	0.015	Bal.

The single-bead deposition was carried out first to investigate the dimensional responses with varying parameters and determine a potential processing window. After processing development, coating and block deposition experiments were performed using the optimized parameters to evaluate the mechanical performance of ER70S-6 parts. The CMT process parameters used in the deposition experiments are given in Table 2. During the coating and block deposition, the overlap rate and layer thickness were fixed at 50% and 3 mm, respectively; the deposited beads were parallel with each other within the same layer while normal to those in adjacent layers. Moreover, during the deposition of a block sample, the Si-enriched particles (also known as silicate islands [13]) on each deposited surface were brushed off layer by layer to investigate their influence on mechanical properties. The sample is therefore denoted by oxide-removal, while the block sample fabricated without this procedure is denoted by as-deposited.

Table 2. Process parameters of CMT-WAAM deposition

	Wire feeding speed, m/min	Travel speed, mm/s
Single-bead	5, 7, 9, 11	10, 15, 20, 25, 30
1 & 2-layer coating	11	30
As-deposited block	11	20
Oxide-removal block	11	20

The deposited samples were removed from substrates and cross-sectioned via electrical discharge machining (EDM) for metallurgical and mechanical characterization. After grinding and polishing, the samples were etched by a 5% Nital etchant for 20 s to reveal the microstructures. An Olympus MX51 optical microscope was used to observe the melt-pool structures. For single-bead and coating samples, the vertical distribution of Vickers hardness was measured every 0.5 mm using a Matsuzawa MMT-X3, with a load force of 200 gf and dwell time of 15 s. For the block samples, a Zwick Roell 8150SK hardness tester was used to measure the Rockwell hardness every 5 mm vertically along the building direction, with a load force of 10 kgf and dwell time of 2 s. An Instron 5982 universal testing machine was used to evaluate the tensile properties according to ASTM E8M-04 standard. The tensile specimens were extracted from both as-deposited and oxide-removal samples, as illustrated in Figure 1. Tensile tests were performed along the deposition direction of specimens with a crosshead speed of 1 mm/min.

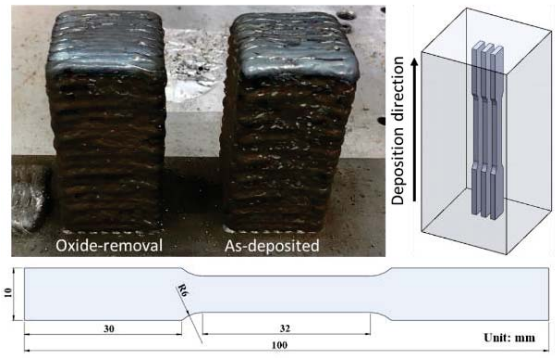

Figure 1. Block samples and the illustration of tensile parts

3. Results and Discussion

3.1 Single-bead dimensions

The single bead is the fundamental element of a CMT-WAAM part, and therefore the understanding of its

dimensional responses to the key CMT parameters, i.e., wire feeding speed (WFS) and travel speed (TS), can help to ensure the efficiency and quality of deposited parts. A processing map including the WFS from 5 to 11 m/min and TS from 10 to 30 mm/s was investigated. The cross-sections with the minimum and maximum areas in the single-bead deposition are shown in Figure 2(a) and (b), along with the illustration showing the measurement of single-bead dimensions, including height (H1), depth (H2), width, and area. Both cross-sections present solid combination between the deposited material and substrate despite their difference in dimensions, suggesting good weldability. The measured dimensions of single-bead cross-sections are plotted in Figure 3(c) to (f). The resultant melt-pool width ranges from 4.94 to 9.06 mm, whilst the height and depth range from 1.14 to 2.73 mm, and 0.67 to 2.35 mm, respectively. Moreover, the cross-section area is distributed between the range of 4.897 to 26.39 mm^2. Overall measured dimensions are positively correlated to the WFS but negatively correlated to the TS. The combination of a high WFS and low TS indicates that more material can be deposited per unit length, therefore, resulting in a large melt pool. Furthermore, the wide dimensional ranges suggest that the single-bead parameters could be optimized according to the geometry of specific components to achieve a balance between deposition efficiency and forming accuracy.

Since the deposition efficiency is the primary consideration of the current CMT-WAAM approach, a wire feeding speed of 11 m/min is selected for the block deposition in this study. The material deposition rate can be estimated by $WFS{\cdot}\rho{\cdot}\pi r^2$, where ρ and r denote the density (7.83 g/cm^3) and radius (0.6 mm) of the ER70S-6 wire, respectively. It should be noted that the practical wire feeding rate is ~8 m/min, rather than the pre-set value (11 m/min) during the deposition. Hence the deposition rate is approximately 4.3 kg/hr, which is significantly higher than those of powder-based AM techniques [6]. It is considered a major advantage of WAAM when applied to repair or produce large metallic components demanded by the marine industry.

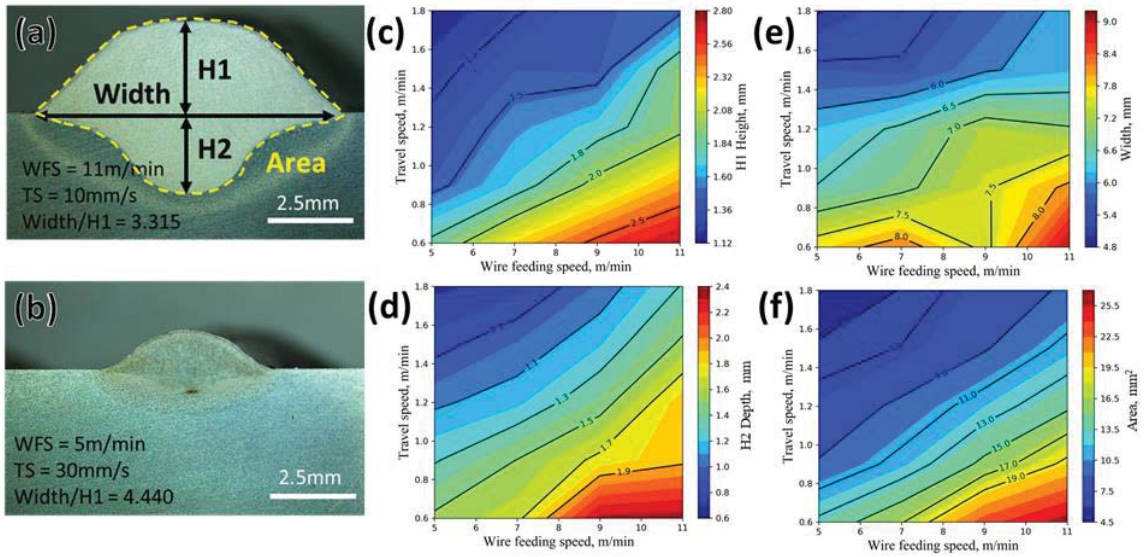

Figure 2. Optical microscopy (OM) images of the (a) maximum and (b) minimum single-bead melt pools. The dimension profiles of measured (c) height, (d) depth, (e) width, and (f) area of melt pools.

3.2 Microstructures

A vertical cross-section of the block fabricated using the optimized parameters is provided in Figure 3(a) The cross-section shows good densification without evident cracking, indicating that successful block formability is achieved by the CMT-WAAM process with the high deposition rate.

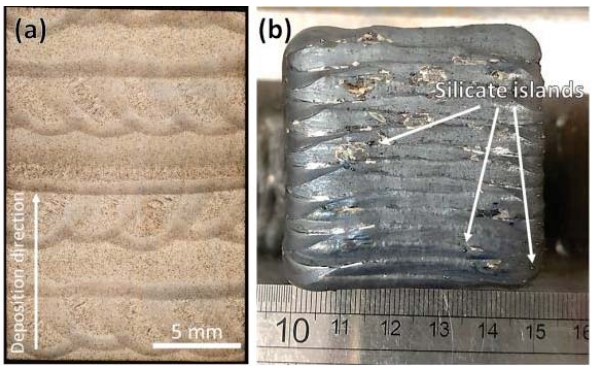

Figure 3. OM image showing the vertical cross-section of the as-deposited block sample. (b) Upper surface of the as-deposited block sample with silicate islands.

Silicate islands are often observed on the weld beads of low-carbon steel with Si as a deoxidizer, and their accumulation may affect the mechanical performance of components composed of multiple beads and layers [13]. Figure 3(b) presents the distribution of evident silicate islands on the as-deposited surface. The microstructures of as-deposited and oxide-removal samples are further revealed in Figure 4(a) and (b). Numerous particles with a diameter of approximately 10 μm are distributed in the as-deposited sample. On the contrary, such obvious particles are rarely observed in the sample with oxide removal. Therefore, the removal of the silicate islands on surfaces can help to reduce the presence of large particles. It indicates that the formation of those large particles in the as-deposited sample is mainly due to the remelting of the silicate islands on layer surfaces. Aside from the large particles, particles smaller than 1 μm are prevalent in both samples, as shown in Figure 4(c). Their diameters are close to two orders of magnitude smaller than the larger particles observed in Figure 4(a). EDS results in Figure 4(c) and (d) show that both the large and small particles are silicate particles, which are comprised of Mn-Si oxides [13].

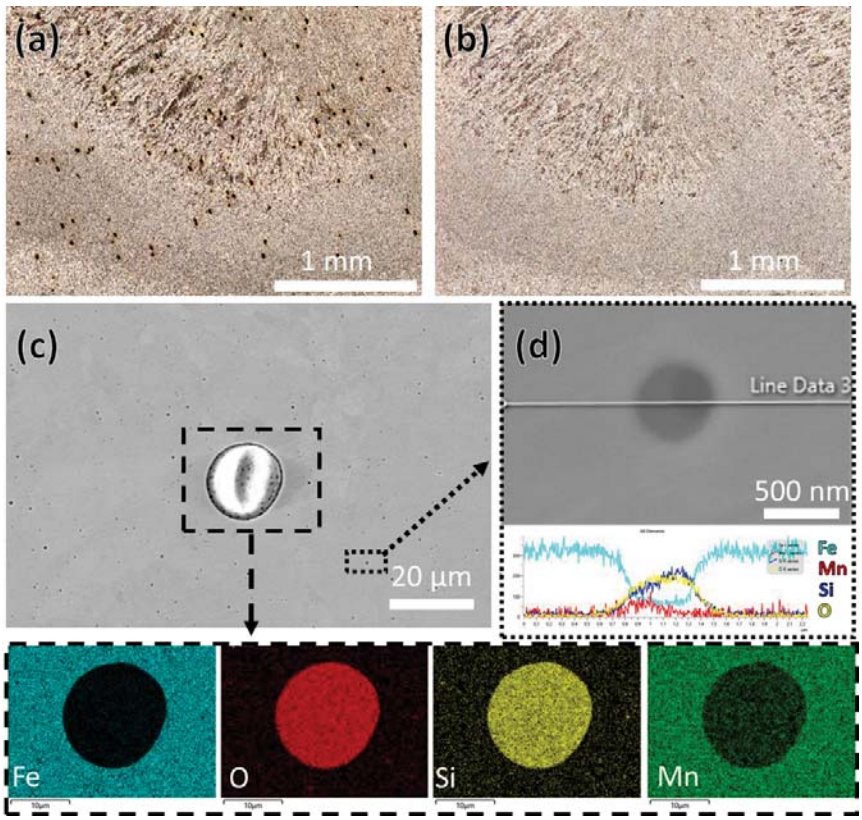

Figure 4. OM images showing the distribution of silicate particles in (a) as-deposited and (b) oxide-removal samples. (c) Scanning electron microscopy (SEM) image of a large silicate particle and corresponding energy dispersive spectroscopy (EDS) mapping results. (d) EDS line scanning result of a small silicate particle.

3.3 Mechanical properties

3.3.1 Hardness

The Vickers hardness distribution of single-bead, 1-layer and 2-layer samples are plotted in Figure 5(a). The hardness of the substrate material is consistent among

different samples. However, the hardness of the as-deposited parts varies with the deposition progress. The single-bead sample possesses the highest hardness (~300 Hv), while the hardness of the 1-layer and 2-layer samples decreases successively. Since hatching was introduced during the deposition of multiple beads and layers, the as-deposited material could undergo remelting and heat input from subsequent beads and layers, i.e., different thermal conditions, leading to the variation of microstructures and resultant mechanical properties [14].

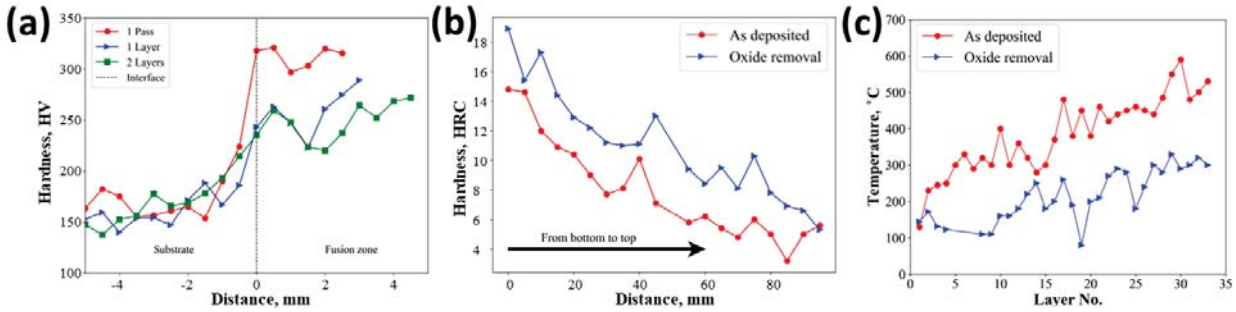

Figure 5. (a) Vertical Vickers hardness distribution of single-bead and coating samples. (b) Vertical Rockwell hardness distribution of as-deposited and oxide-removal samples. (c) Surface temperature profiles during the block deposition of as-depositedand oxide-removal samples.

The Rockwell hardness results of the block samples are plotted in Figure 5(b), and the hardness measured at the top and bottom are given in Table 3. The hardness of both samples shows a significant decreasing trend from bottom to top, and the hardness of the sample with oxide removal is overall higher than that of the as-deposited sample. During the deposition of the block samples, the heat accumulation is substantial and results in increasing surface temperatures layer by layer. Consequently, the top part solidifies under a relatively low cooling rate while the bottom part experiences prolonged heat input. Similar mechanical heterogeneity has been recognized in AMed parts produced with different materials and techniques [15]. To monitor the temperature variations during block deposition, the surface temperature was measured before the deposition of each layer, and the results are plotted in Figure 5(c). Besides the layer-wise increment of temperatures, it is recognized that the surface temperature of the sample with oxide removal is overall lower due to the increased holding time between layers. The interlayer holding time was fixed at 30 s during the deposition of the as-deposited sample but increased over 30 s due to the oxide-removal operation. Therefore, the thermal histories experienced by the as-deposited and oxide-removal samples were different and could be the key factor in mechanical properties aside from the Si-rich particles.

Table 3. Mechanical properties of as-deposited and oxide-removal samples

	As-deposited	Oxide-removal	GMAW (vertical)
Hardness at bottom, HRC	14.8	18.9	3 – 6
Hardness at top, HRC	5.6	5.3	
Yield strength, MPa	348.8	394.0	396 ± 26
Ultimate tensile strength, MPa	504.0	540.0	503 ± 21
Fracture elongation, %	24.8	20.3	12 ± 3

3.3.2 Tensile properties

The mechanical properties of block samples were also evaluated by tensile tests. The stress-strain curves are plotted in Figure 6(a), and the yield strength, ultimate tensile strength and fracture elongation results are given in Table 3. In accordance with the hardness results, the sample with oxide removal possesses enhanced strength. Meanwhile, there is also concomitant decay of ductility as the strength improves, showing a strength-ductility trade-off. The fractography in Figure 6(b) and (c) suggests that the early failure tends to occur around the large silicate particles in both samples. Although Figure 4(b) shows that such large particles can be significantly removed, there are still residual ones which limit the ductility of the sample with oxide removal. On the other hand, the size of the large silicate particles is too large for effective dispersion strengthening [16].

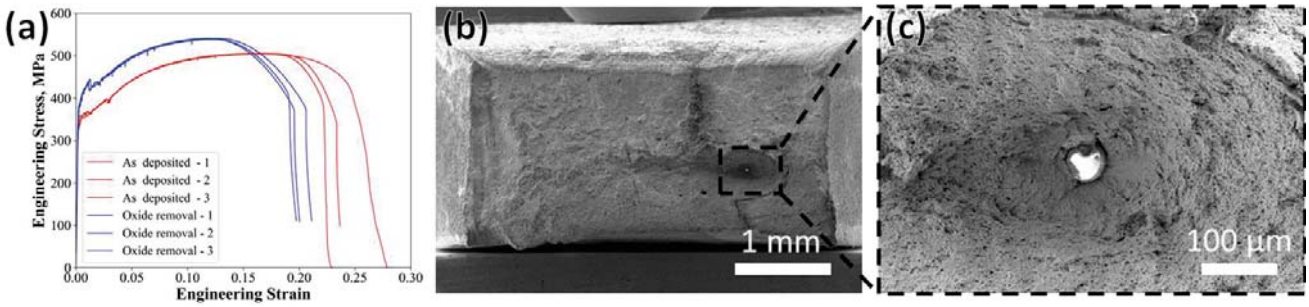

Figure 6. (a) Tensile curves of as-deposited and oxide-removal samples. (b) SEM fractography of an oxide-removal sample and (c) a large silicate particle revealed at its fracture surface.

In general, the ER70S-6 parts produced by the current CMT approach possess comparable tensile strength and hardness against the one produced by GMAW-WAAM, as shown in Table. 3 [10]. The microhardness distribution and tensile results further suggest that the mechanical performance of ER70S-6 is sensitive to the thermal history during deposition, whilst the influence of the amount of silicate islands on the mechanical properties is modest.

4. Conclusions

In this study, ER70S-6 was successfully deposited by the CMT-WAAM process with a high deposition rate. The wide range of the attainable output bead dimensions suggests that further processing optimization could be carried out to balance the efficiency and accuracy of the process. The silicate islands that occurred on deposited surfaces could be partially removed during the printing process to reduce the number of large silicate particles in the block sample. However, such large particles cannot be fully eliminated and therefore limit the ductility of both as-deposited and oxide-removal samples. The thermal evolution during the AM process has a more significant influence on the mechanical performance of WAAMed ER70S-6, than the amount of large silicate particles. Hence, it is important to control the dwell time between layers to fabricate components with consistent mechanical performances.

5. Acknowledgements

This research was supported by Agency for Science, Technology and Research (A*Star), Republic of Singapore, under the IAF-ICP program, “Development of advanced laser aided additive manufacturing (LAAM) & hybrid laser-arc welding (HLAW) technologies for complex marine & offshore structures”, Grant No: I2001E0074

6. References

1. B. Blakey-Milner et al., “Metal Additive Manufacturing in Aerospace: A Review,” Mater. Des., Vol. 209, p. 110008, 2021.
2. J. Donoghue, A. A. Antonysamy, F. Martina, P. A. Colegrove, S. W. Williams, and P. B. Prangnell, “The Effectiveness of Combining Rolling Deformation with Wire–Arc Additive Manufacture on β-Grain Refinement and Texture Modification in Ti–6Al–4V,” Mater. Charact., Vol. 114, pp. 103–114, 2016.
3. D. Gu, “Laser Additive Manufacturing (AM):

Classification, Processing Philosophy, and Metallurgical Mechanisms," in Laser Additive Manufacturing of High-Performance Materials, D. Gu, Ed. Berlin, Heidelberg: Springer Berlin Heidelberg, pp. 15–71, 2015.

4. N. Kumar et al., "Wire Arc Additive Manufacturing – A Revolutionary Method in Additive Manufacturing," Mater. Chem. Phys., Vol. 285, p. 126144, 2022.

5. S. Selvi, A. Vishvaksenan, and E. Rajasekar, "Cold Metal Transfer (CMT) Technology - An Overview," Def. Technol., Vol. 14, No. 1, pp. 28–44, 2018.

6. R. M. Kindermann, M. J. Roy, R. Morana, and P. B. Prangnell, "Process Response of Inconel 718 to Wire + Arc Additive Manufacturing with Cold Metal Transfer," Mater. Des., Vol. 195, p. 109031, 2020.

7. C. Zhang, Y. Li, M. Gao, and X. Zeng, "Wire Arc Additive Manufacturing of Al-6Mg Alloy Using Variable Polarity Cold Metal Transfer Arc as Power Source," Mater. Sci. Eng. A, Vol. 711, pp. 415–423, 2018.

8. Ron, Levy, Dolev, Leon, Shirizly, and Aghion, "Environ mental Behavior of Low Carbon Steel Produced by a Wire Arc Additive Manufacturing Process," Metals, Vo l. 9, No. 8, p. 888, 2019.

9. C. V. Haden, G. Zeng, F. M. Carter, C. Ruhl, B. A. Krick, and D. G. Harlow, "Wire and Arc Additive Manufactured Steel: Tensile and Wear Properties," Addit. Manuf., Vol. 16, pp. 115–123, 2017.

10. M. Rafieazad, M. Ghaffari, A. Vahedi Nemani, and A. Nasiri, "Microstructural Evolution and Mechanical Properties of A Low-Carbon Low-Alloy Steel Produced by Wire Arc Additive Manufacturing," Int. J. Adv. Manuf. Technol., Vol. 105, No. 5–6, pp. 2121–2134, 2019.

11. N. Sridharan, M. W. Noakes, A. Nycz, L. J. Love, R. R. Dehoff, and S. S. Babu, "On The Toughness Scatter in Low Alloy C-Mn Steel Samples Fabricated Using Wire Arc Additive Manufacturing," Mater. Sci. Eng. A, Vol. 713, pp. 18–27, 2018.

12. A. Ermakova, A. Mehmanparast, S. Ganguly, J. Razavi, and F. Berto, "Fatigue Crack Growth Behaviour of Wire and Arc Additively Manufactured ER70S-6 Low Carbon Steel Components," Int. J. Fract., Vol. 235, pp. 47–59, 2022.

13. American Welding Society, R. Derrien, E. M. Sullivan, S. Liu, E. Moine, and F. Briand, "Silicate Island Formation in Gas Metal Arc Welding," Weld. J., Vol. 100, No. 01, pp. 13–26, 2021.

14. C. R. Cunningham, J. M. Flynn, A. Shokrani, V. Dhokia, and S. T. Newman, "Invited Review Article: Strategies and Processes for High Quality Wire Arc Additive Manufacturing," Addit. Manuf., Vol. 22, pp. 672–686, 2018.

15. Y. Kok et al., "Anisotropy and Heterogeneity of Microstructure and Mechanical Properties in Metal Additive Manufacturing: A Critical Review," Mater. Des., Vol. 139, pp. 565–586, 2018.

16. Z. Zhang and D. L. Chen, "Contribution of Orowan Strengthening Effect in Particulate-Reinforced Metal Matrix Nanocomposites," Mater. Sci. Eng. A, Vol. 483–484, pp. 148–152, 2008.